Electronic Supplementary Information (ESI)

Luminescent Polymorphic Aggregates of Trinuclear Cu(I)-pyrazolate Tuned by Intertrimeric Cu···N_{Py} Weak Coordination Bonds

Shun-Ze Zhan,*[a] Wei Chen,[a] Ji Zheng,[b] Seik Weng Ng[c] and Dan Li *[b]

[a] *Department of Chemistry and Key Laboratory for Preparation and Application of Ordered Structural Materials of Guangdong Province, Shantou University, Shantou 515063, P. R. China* *Email: szzhan@stu.edu.cn

[b] *College of Chemistry and Materials Science, and Guangdong Provincial Key Laboratory of Functional Supramolecular Coordination Materials and Applications, Jinan University, Guangzhou 510632, P. R. China* *Email: danli@jnu.edu.cn

[c] *UCSI University, 56000 Cheras, Kuala Lumpur, Malaysia*

Content

Section 1: Experimental Section

1.1 Materials and Physical Measurements

Commercially available chemicals were purchased and used without further purification. Infrared spectra were obtained in KBr disks on a Nicolet Avatar 360 FTIR spectrometer in the range of 4000-400 cm^{-1}. Elemental analyses of C, H and N were determined with the instrument Elementar Vario EL III CHNS analyzer. Thermogravimetric analysis (TGA) were performed on a TA Instruments Q50 Thermogravimetric Analyzer under nitrogen flow of (40 $mL \cdot min^{-1}$) at a typical heating rate of 10 $°C \cdot min^{-1}$. X-Ray power diffraction (XRPD) experiments were performed on a D8 Advance X-ray diffractometer.

The solid-state diffuse reflectance UV-Vis spectra were recorded on a Lambda950 UV/Vis/NIR spectrophotometer of Perkin Elmer using pure powder sample. The steady-state photoluminescence spectra (PL) for all samples were recorded at temperature range from 77 K to 375 K on a PTI QM/TM spectrofluorometer (Birmingham, NJ, USA). Corrections of excitation and emission for the detector response were performed ranging from 200-900 nm. Lifetime measurements were measured by a single photon counting spectrometer on an Edinburgh FLS920 spectrometer equipped with a μF900 microsecond flash lamp, a red-sensitive Peltier-cooled Hamamatsu R928P photomultiplier tube (PMT). The data were analyzed by iterative convolution of the luminescence decay profile with the instrument response function using the software package provided by Edinburgh Instruments. The crystal phase purity of the samples were assured by elemental analysis and X-ray powder diffraction measurements.

1.2 Synthesis

Complex [*anti*-$Cu_3L_3]_2$ (1) A mixture of *H***L** (10.2 mg, 0.05 mmol), $Cu(NO_3)_2 \cdot 3H_2O$ (24.4 mg, 0.1 mmol), C_2H_5OH (3.0 mL) and aqueous $NH_3 \cdot H_2O$ (100 μL) was sealed in a 8.0 mL Pyrex tube and heated at 140 ºC in an oven for 72 h, then slowly cooled at a rate of –5 $°C \cdot h^{-1}$ to room temperature. Colorless needle-like crystals

were obtained. Anal. Calcd for $C_{30}H_{30}Cu_3N_9S_3$: C 44.85, H 3.76, N 15.69, S 11.97 %. Found: C 44.86, H 4.06, N 15.74, S12.05 %. IR data (KBr, cm^{-1}): 2924 w, 2851 w, 1636 vs, 1573 vs, 1478 m, 1482 m, 1415 m, 1105 m, 808 m ,700 s.

Complex [*syn*-$Cu_3L_3 \cdot C_2H_5OH]_2$ (2) A mixture of H**L** (10.2 mg, 0.05 mmol), $Cu(NO_3)_2 \cdot 3H_2O$ (24.4 mg, 0.1 mmol), C_2H_5OH (3.0 mL) and aqueous $NH_3 \cdot H_2O$ (20 μL) was sealed in a 8.0 mL Pyrex tube and heated in an oven at 140 ºC for 72 h, then slowly cooled at a rate of –5 °C·h^{-1} to room temperature. The tube was set aside for 7 days without perturb then colorless sheet-like crystals were obtained with little yielding. Anal. Calcd for $C_{32}H_{36}Cu_3N_9S_3O$: C 45.05, H 4.02, N 15.25, S 11.64 %. Found: C 44.96, H 4.16, N 15.44, S11.85 %. IR data (KBr, cm^{-1}): 3446 vs, 2917 w, 1637 vs, 1599 vs ,1569 vs, 1480 m, 1420 m, 1105w, 1054 w, 804 w, 706 s.

Complex [*anti*-$Cu_3L_3 \cdot C_2H_5OH]_n$ (3) A mixture of H**L** (10.2 mg, 0.05 mmol), $Cu(NO_3)_2 \cdot 3H_2O$ (24.4 mg, 0.1 mmol), C_2H_5OH (3.0 mL) and aqueous $NH_3 \cdot H_2O$ (60 μL) was sealed in a 8.0 mL Pyrex tube and heated at 140 ºC in an oven for 72 h, then slowly cooled at a rate of –5 °C·h^{-1} to room temperature. Light-green block crystals were obtained. Anal. Calcd for $C_{32}H_{36}Cu_3N_9S_3O$: C 45.05, H 4.02, N 15.25, S 11.64 %, Found: C45.23, H 3.99, N 15.13, S 11.78 %. IR data (KBr, cm^{-1}): 3450 vs, 2956 w, 2914 w, 1636 w, 1573 vs, 1481 m, 1402 m, 1479 vs, 1215 s, 1102 s, 804 m, 710 w.

Complex [*anti*-$Cu_3L_3 \cdot 0.5C_7H_8]_n$ (4) A mixture of H**L** (10.2 mg, 0.05 mmol), $Cu(ClO_4)_2 \cdot 6H_2O$ (37.0 mg, 0.1 mmol), ethanol (1.5 mL), toluene (1.5 mL) and aqueous $NH_3 \cdot H_2O$ (60 μL) were sealed in a 8.0 mL Pyrex tube and heated at 140 ºC in an oven for 72 h, then slowly cooled at a rate of –5 °C·h^{-1} to room temperature. Yellowish-green block-like crystals were obtained. Anal. Calcd for $C_{33.5}H_{34}Cu_3N_9S_3$: C 47.36, H 4.03, N 14.84, S 11.32 %, Found: C 47.57, H 3.89, N 14.93, S 11.20 %. IR data (KBr, cm^{-1}): 2955 s, 2908 w, 1628 w, 1575 vs, 1477 m, 1411 m, 1366 w, 1336 w, 1105 w, 810 m, 703 w.

Complex [*syn*-$Cu_3L_3 \cdot C_8H_{10}]_n$ (5) A mixture of H**L** (10.2 mg, 0.05 mmol), $CuCl_2 \cdot 2H_2O$ (17 mg, 0.1 mmol), ethanol (1.5 mL), *o*-xylene (1.5 mL) and aqueous $NH_3 \cdot H_2O$ (60 μL) was sealed in a 8.0 mL Pyrex tube and heated at 140 ºC in an oven for 72 h, then slowly cooled at a rate of –5 °C·h^{-1} to room temperature. Light-yellow crystals were obtained. Anal. Calcd for $C_{38}H_{40}Cu_3N_9S_3$: C 50.18, H 4.43, N 13.86, S 10.58 %, Found: C 50.06, H 4.53, N 13.62, S 10.62 %. IR data (KBr, cm^{-1}): 2914 w, 2848 s, 1572 vs, 1539 w, 1491 m, 1402 m, 1310 w, 1206 m, 1102 w, 977 m, 736 w, 706 m.

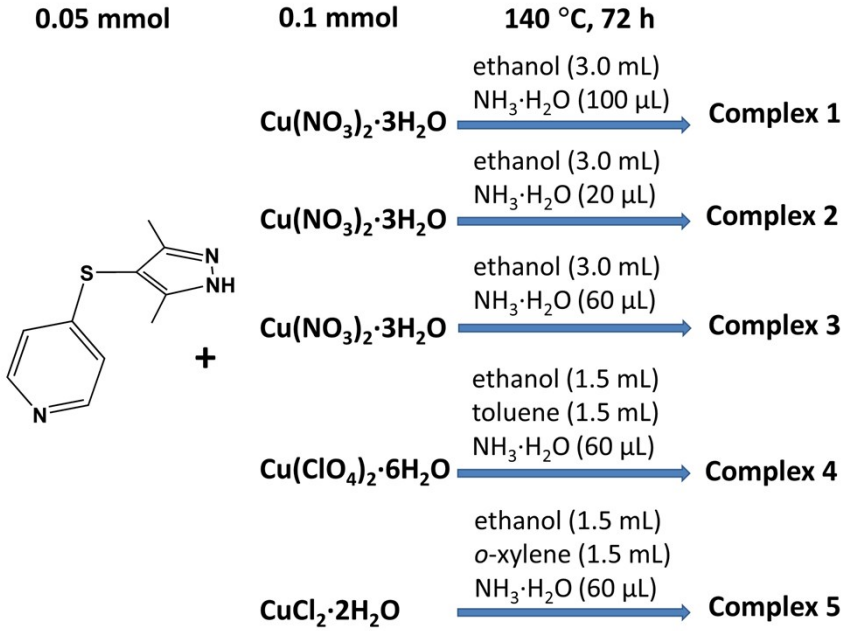

Scheme S1 Synthesis procedure of the complexes **1**-**5**.

Caution! In the synthesis of these complexes, the volume of solution should not exceed one half of the volume of the Pyrex tube to avoid overloading. Be careful of avoiding potential empyrosis and catching fire when flame-sealing. Be careful of potential explosive of copper(II) hyperchlorate.

Section 2: Crystal Data and Additional Structural Description

2.1 Crystal Structure Determination

Suitable crystals were mounted with glue at the end of a glass fiber. Single crystal data were collected on an Oxford Diffraction Gemini E (Enhance Mo X-Ray source, Kα, λ = 0.71073 Å) equipped with a graphite monochromator and ATLAS CCD detector (CrysAlis CCD, Oxford Diffraction Ltd) under the cold nitrogen stream (100 K). The data was processed using CrysAlis RED, Oxford Diffraction Ltd (Version 1.171.34.44, release 25-10-2010 CrysAlis171.NET). Multi-scan absorptions were applied. Structure were solved by direct methods (SHELXTL-97) and refined on F^2 using full-matrix least-squares (SHELXTL-97).[S1] All non-hydrogen atoms were refined with anisotropic thermal parameters, and all hydrogen atoms were included in calculated positions and refined with isotropic thermal parameters riding on the parent atoms. The thermal ellipsoid diagrams were produced by ORTEP-3. Structural diagrams were produced by using the OLEX computer program. Crystal data and structure refinement for these complexes are summarized in Table S1. Selected bond lengths and angles are given in Table S2. CCDC nos. 1855939-1855943 contain the supplementary crystallographic data for this paper.

2.2 Crystal Data

Table S1 Crystal data and structure refinement parameters of the complexes **1–5** at 100 K

Parameter	**1**	**2**	**3**	**4**	**5**
CCDC	1855939	1855940	1855941	1855942	1855943
Chemical formula	$C_{30}H_{30}Cu_3N_9S_3$	$C_{32}H_{36}Cu_3N_9S_3O$	$C_{32}H_{36}Cu_3N_9S_3O$	$C_{33.5}H_{34}Cu_3N_9S_3$	$C_{38}H_{40}Cu_3N_9S_3$
Formula weight	803.43	849.50	849.50	849.50	909.59
Crystal system	Triclinic	Triclinic	Triclinic	Triclinic	Triclinic
Space group	*P*-1	*P*-1	*P*-1	*P*-1	*P*-1
a (Å)	5.5976(6)	10.7852(9)	10.0630(3)	10.0679(3)	11.7467(8)
b (Å)	15.2435(16)	11.6669(9)	12.0715(3)	12.1410(4)	14.2967(11)
c (Å)	20.009(2)	16.0438(14)	14.8898(4)	14.9936(5)	14.4607(11)
α (deg)	69.029(10)	99.756(7)	102.747(2)	103.592(3)	117.989(8)
β (deg)	87.551(9)	91.267(7)	97.489(2)	98.639(3)	93.212(6)
γ (deg)	88.214(8)	115.760(8)	93.497(2)	92.783(3)	111.492(7)
V (Å^3)	1592.5(3)	1781.4(3)	1741.57(8)	1754.48(10)	1917.0(3)
Z	2	2	2	2	2
D_{Calcd} (g·cm^{-3})	1.675	1.584	1.620	1.608	1.576
μ (mm^{-1})	2.220	1.991	2.037	2.020	1.854
Reflns collected	9072	12469	14430	14901	17904
Unique reflns	5531	7328	7725	7801	8561
R_{int}	0.0797	0.0671	0.0238	0.0197	0.0592
GOF	1.083	1.007	1.030	1.036	1.088
R_1 [a] [I > 2σ(I)]	0.0918	0.0700	0.0287	0.0285	0.0757
wR_2 [b] [I > 2σ(I)]	0.1677	0.1035	0.0660	0.0689	0.1881
R_1 [a] [all refl.]	0.1534	0.1419	0.0369	0.0337	0.1159
wR_2 [b] [all refl.]	0.1956	0.1301	0.0697	0.0716	0.2101

[a] $R_1 = \sum(||F_0| - |F_c||)/\sum|F_0|$. [b] $wR_2 = [\sum w(F_0^2 - F_c^2)^2/\sum w(F_0^2)^2]^{1/2}$.

Table S2 Selected bond lengths (Å) and angles (°) of the complexes **1-5**

Bond lengths		Bond angles	
Complex 1			
Cu(1)-N(1)	1.860(8)	N(1)-Cu(1)-N(8)	173.5(3)
Cu(1)-N(8)	1.863(8)	N(2)-Cu(2)-N(4)	178.1(4)
Cu(2)-N(2)	1.861(7)	N(5)-Cu(3)-N(7)	176.0(3)
Cu(2)-N(4)	1.861(7)	N(1)-Cu(1)-N(9)#1	90.9(1)
Cu(3)-N(5)	1.831(8)	N(8)-Cu(1)-N(9)#1	95.3(1)
Cu(3)-N(7)	1.851(9)		
Cu(1)-N(9)#1	2.670 (2)		
Symmetry codes: #1 -x+1, -y+2, -z+1			
Complex 2			
Cu(1)-N(1)	1.909(5)	N(1)-Cu(1)-N(8)	169.2(2)
Cu(1)-N(8)	1.902(5)	N(2)-Cu(2)-N(4)	170.9(2)
Cu(2)-N(2)	1.847(5)	N(5)-Cu(3)-N(7)	175.6(2)
Cu(2)-N(4)	1.855(5)	N(8)-Cu(1)-N(3)#1	96.6(2)
Cu(3)-N(5)	1.848(5)	N(1)-Cu(1)-N(3)#1	94.1(2)
Cu(3)-N(7)	1.853(5)		
Cu(1)-N(3)#1	2.308(5)		
Symmetry codes: #1 -x+1, -y, -z+1			
Complex 3			
Cu(1)-N(1)	1.858(1)	N(1)-Cu(1)-N(8)	176.7(4)
Cu(1)-N(8)	1.857(5)	N(2)-Cu(2)-N(4)	163.0(1)
Cu(2)-N(2)	1.896(3)	N(5)-Cu(3)-N(7)	172.9(3)
Cu(2)-N(4)	1.890(9)	N(2)-Cu(2)-N(3)#1	99.2(1)
Cu(3)-N(5)	1.873(8)	N(4)-Cu(2)-N(3)#1	97.6(5)
Cu(3)-N(7)	1.876(5)	N(5)-Cu(3)-N(6)#2	94.3(9)
Cu(2)-N(3)#1	2.357(2)	N(7)-Cu(3)-N(6)#2	92.6(5)
Cu(3)-N(6)#2	2.495(2)		
Symmetry codes: #1 -x+1, -y+1, -z+1; #2 -x+1, -y+1, -z+2;			

Complex 4			
Cu(1)-N(1)	1.852(7)	N(1)-Cu(1)-N(8)	176.7(5)
Cu(1)-N(8)	1.855(9)	N(2)-Cu(2)-N(4)	162.6(2)
Cu(2)-N(2)	1.898(2)	N(5)-Cu(3)-N(7)	170.8(4)
Cu(2)-N(4)	1.895(2)	N(2)-Cu(2)-N(3)#1	99.0(4)
Cu(3)-N(5)	1.874(2)	N(4)-Cu(2)-N(3)#1	98.2(3)
Cu(3)-N(7)	1.873(4)	N(5)-Cu(3)-N(6)#2	95.4(1)
Cu(2)-N(3)#1	2.326(2)	N(7)-Cu(3)-N(6)#2	93.7(6)
Cu(3)-N(6)#2	2.416(8)		
Symmetry codes: #1 -x+1, -y+1, -z; #2 -x+1, -y+1, -z+1			
Complex 5			
Cu(1)-N(1)	1.886(5)	N(1)-Cu(1)-N(8)	171.8(2)
Cu(1)-N(8)	1.879(5)	N(2)-Cu(2)-N(4)	173.3(2)
Cu(2)-N(2)	1.888(5)	N(5)-Cu(3)-N(7)	168.1(2)
Cu(2)-N(4)	1.880(5)	N(1)-Cu(1)-N(9) #1	95.8(2)
Cu(3)-N(5)	1.873(6)	N(8)-Cu(1)-N(9) #1	92.4(2)
Cu(3)-N(7)	1.880(6)	N(2)-Cu(2)-N(3) #2	91.9(2)
Cu(1)-N(9)#1	2.461(6)	N(4)-Cu(2)-N(3)#2	94.6(1)
Cu(2)-N(3)#2	2.530(7)	N(5)-Cu(3)-N(6)#3	98.9(1)
Cu(3)-N(6)#3	2.519(8)	N(7)-Cu(3)-N(6)#3	92.5(4)
Symmetry codes: #1-x+1, -y+1, -z; #2 –x+2, -y+2, -z+1; #3 -x+2, -y+2,-z			

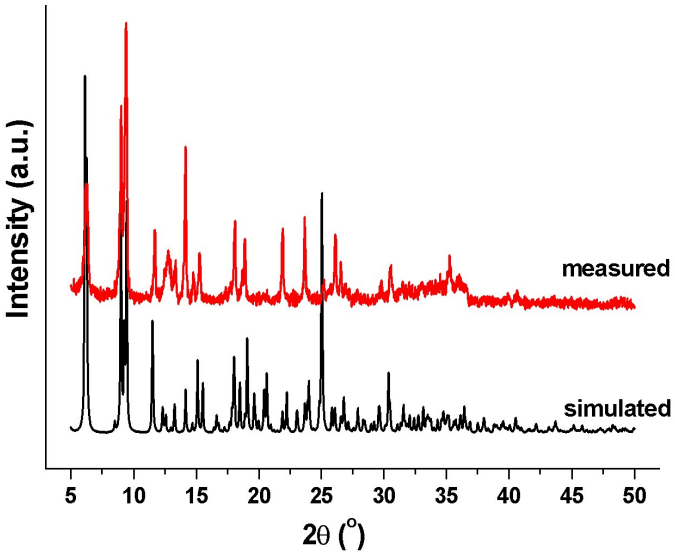

(a) Complex **1**

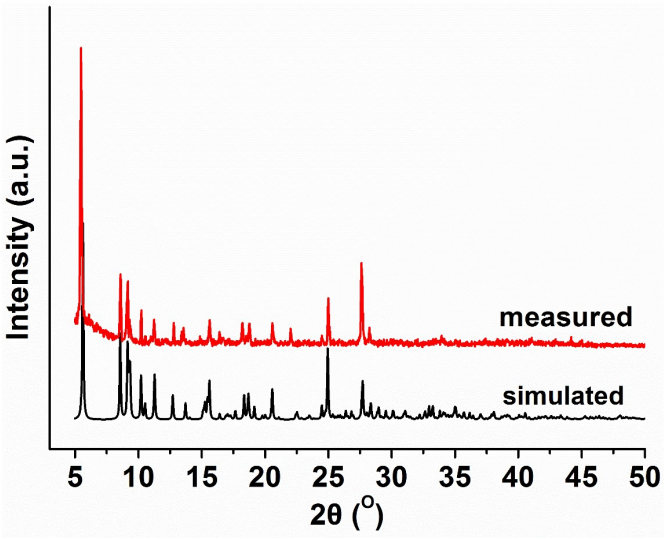

(b) Complex **2**

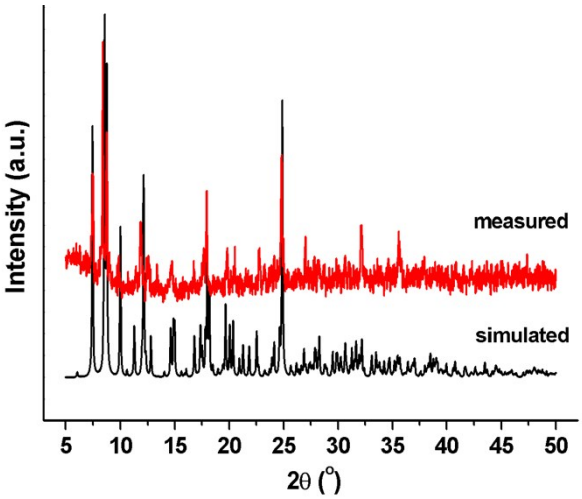

(c) Complex **3**

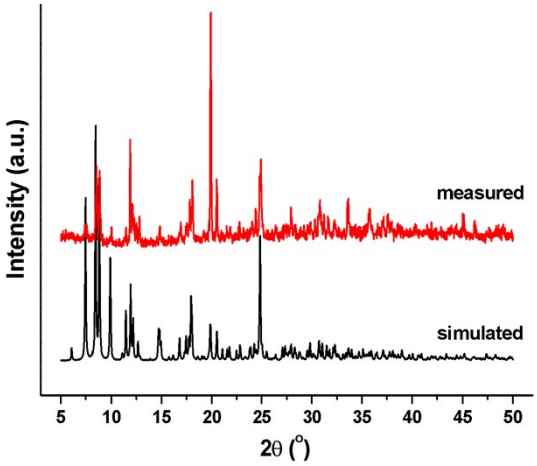

(d) Complex **4**

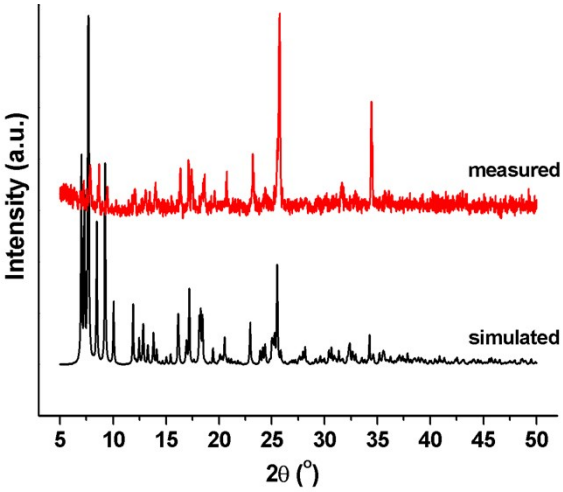

(d) Complex **5**

Fig. S1 Comparison of measured and simulated PXRD patterns of the complex **1-5**.

2.2 Additional Structural Description

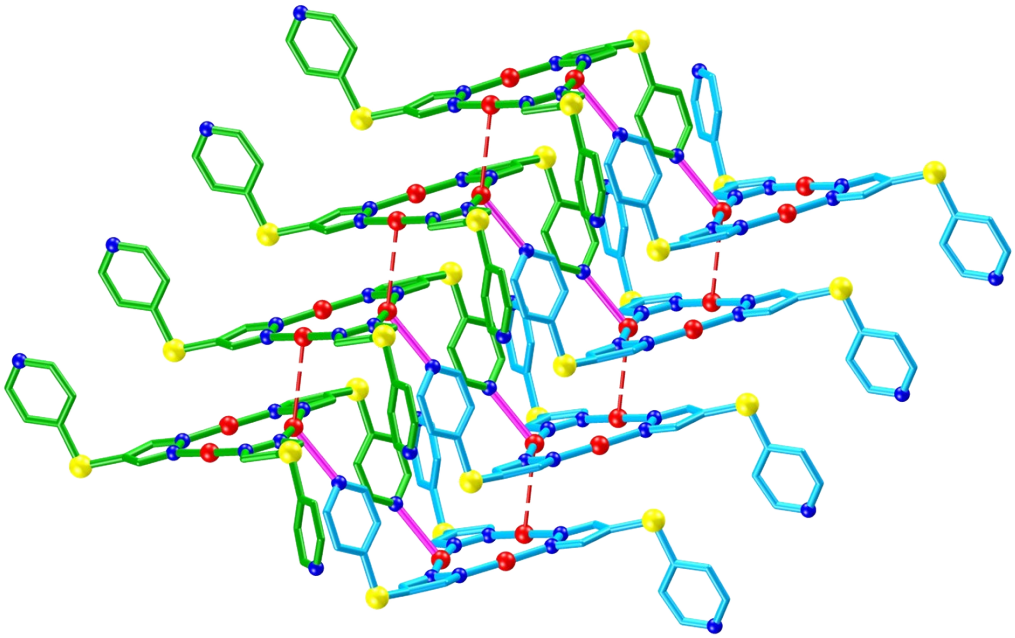

(a) Chain-like aggregates supported by intertrimeric $N_{Py}\cdots Cu$ weak coordination bonds (purple bond) and Cu···Cu (red dotted bond) weak interactions

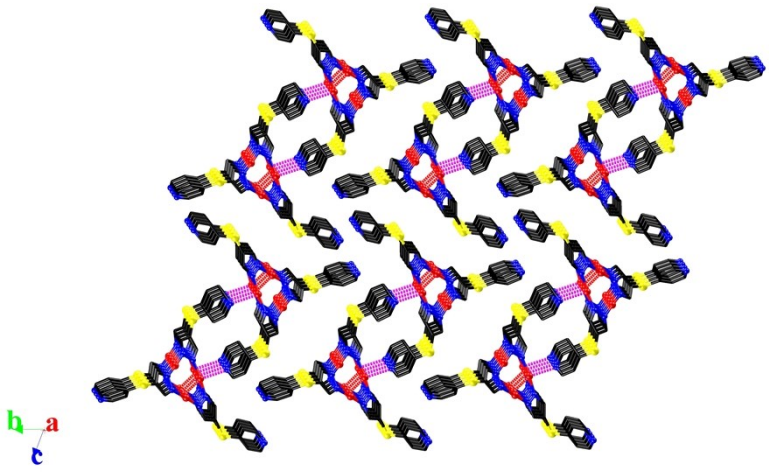

(b) Packing diagram along *a* axis

Fig. S2 Structural diagram of the complex **1** to show polymeric aggregates. All methyl groups and H atoms are omitted for clarity.

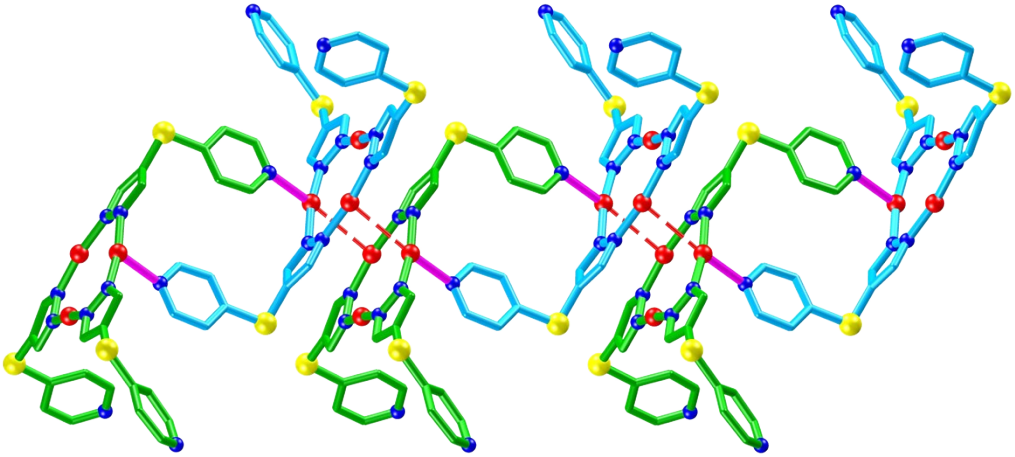

(a) Chain-like aggregates supported by intertrimeric $N_{Py}\cdots Cu$ (purple bond) weak coordination bonds and Cu···Cu (red dotted bond) weak interactions

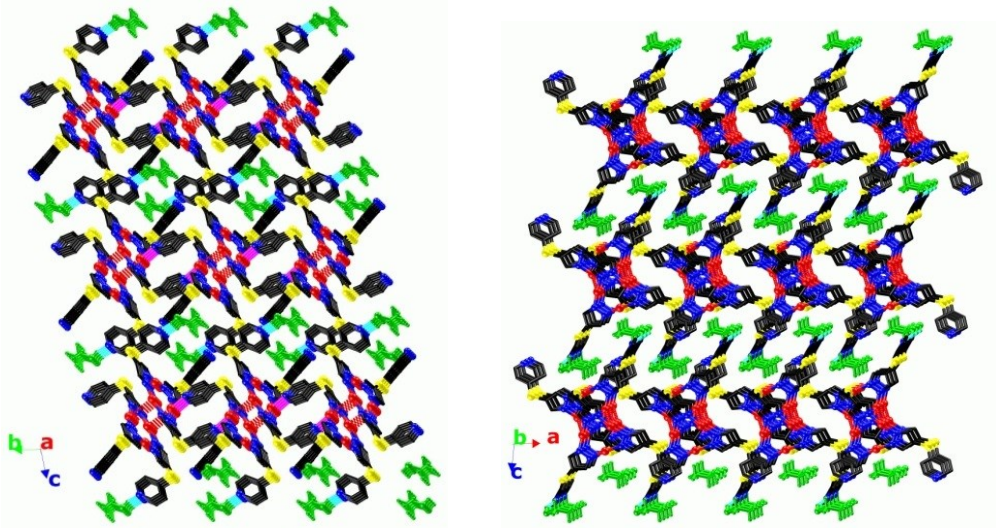

(c) Packing diagram along *a* (left) and *b* (right) axis showing crystallized ethanol molecules (green color) attached on pyridyl groups by O-H···N hydrogen bonds (Cyan dotted bond).

Fig. S3 Structural diagram of the complex **2** to show polymeric aggregates. All methyl groups and H atoms are omitted for clarity except in ethanol molecules.

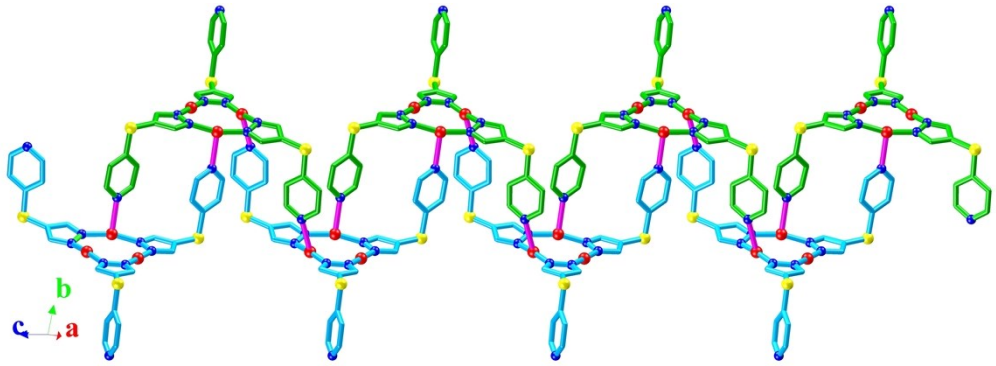

(a) Chain-like aggregates supported by intertrimeric $N_{Py}\cdots Cu$ weak coordination bonds (purple bond) weak interactions

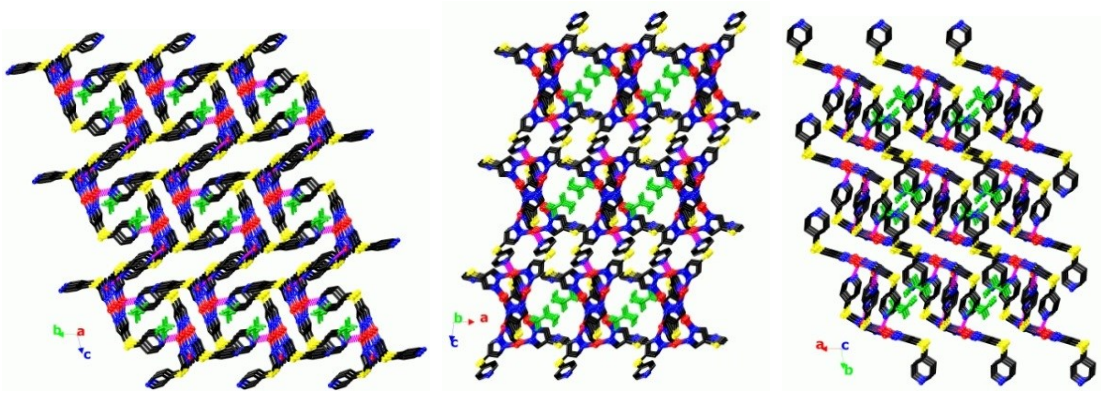

(b) Packing diagram along *a* (left), *b* (middle) and *c* (right) axis showing crystallized ethanol molecules (green color) ocuppied the vacant space.

Fig. S4 Structural diagram of the complex **3** to show polymeric aggregates. All methyl groups and H atoms are omitted for clarity except in ethanol molecules.

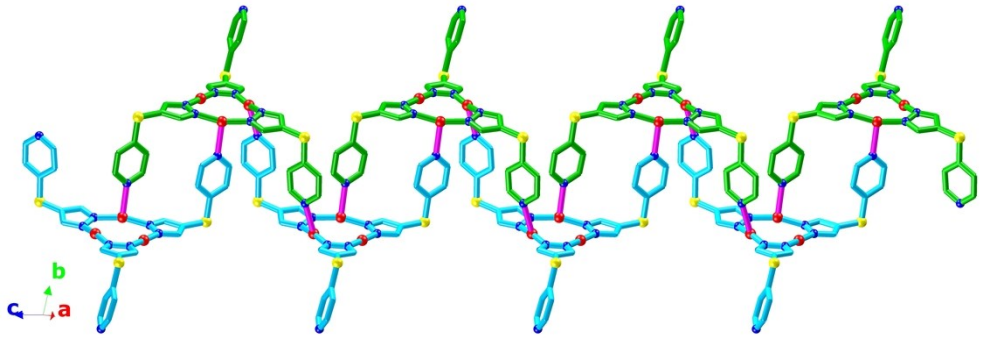

(a) Chain-like aggregates supported by intertrimeric $N_{Py}\cdots Cu$ (purple bond) weak interactions

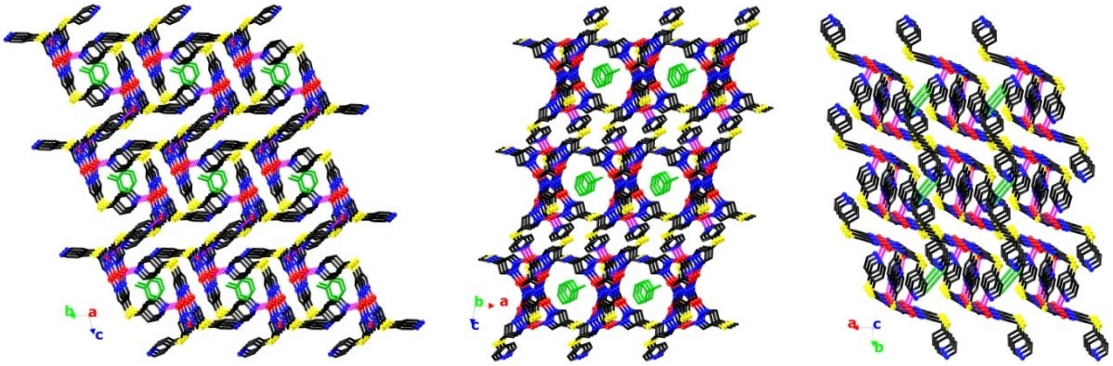

(b) Packing diagram along *a* (left), *b* (middle) and *c* (right) axis showing crystallized toluene molecules (green color) ocuppied the vacant space.

Fig. S5 Structural diagram of the complex **4** to show polymeric aggregate. All H atoms and methyl groups in **L** are omitted for clarity.

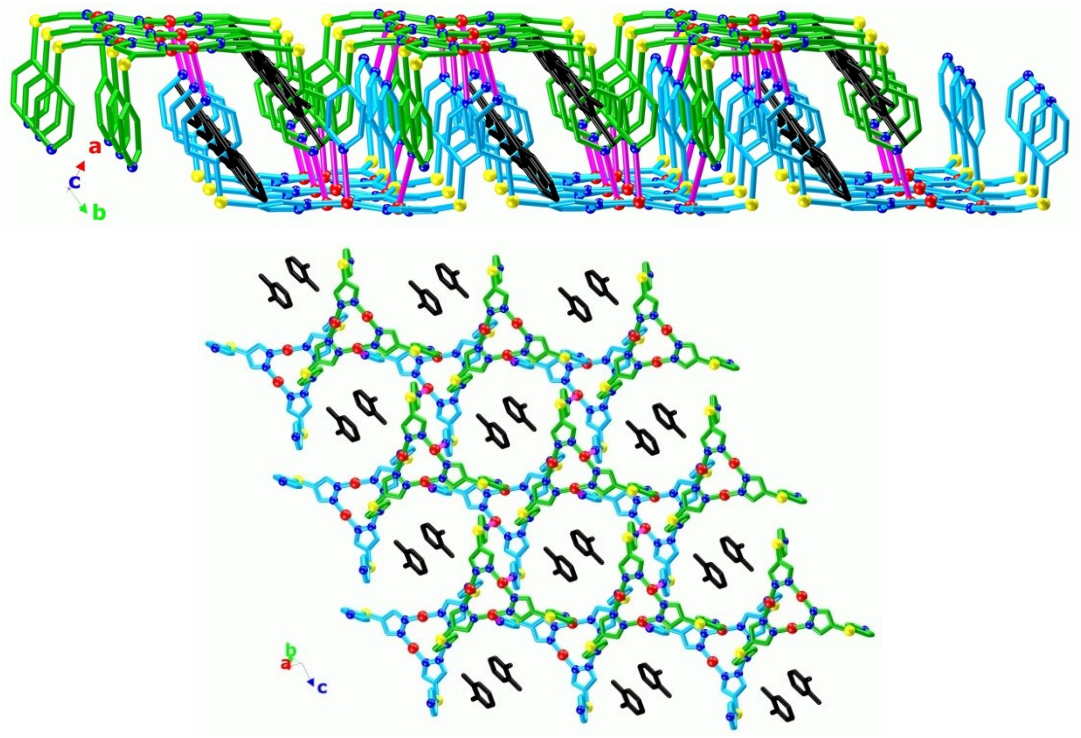

(a) Single layer from side (top) and top (bottom) view showing vacant spaces are ocupied by *o*-xyelene molecules (black).

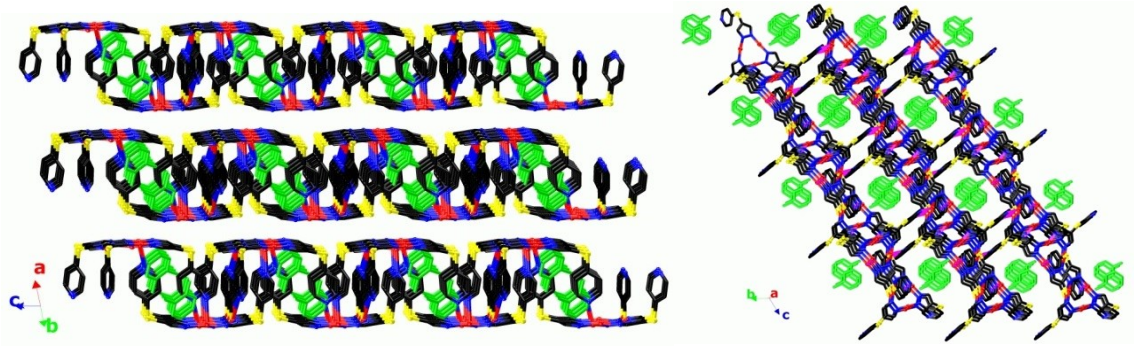

(b) Packing diagram from side (top) and top (bottom) view

Fig. S6 Structural diagram of the complex **5** to show 2-D polymeric aggregate. All H atoms and methyl groups in **L** are omitted for clarity.

Section 3: Thermal stabilities and crystal transformation

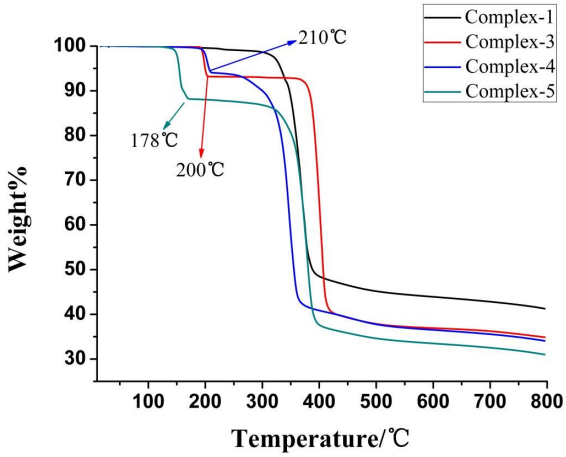

Fig. S7 TGA curves of the complexes **1** and **3**-**5**.

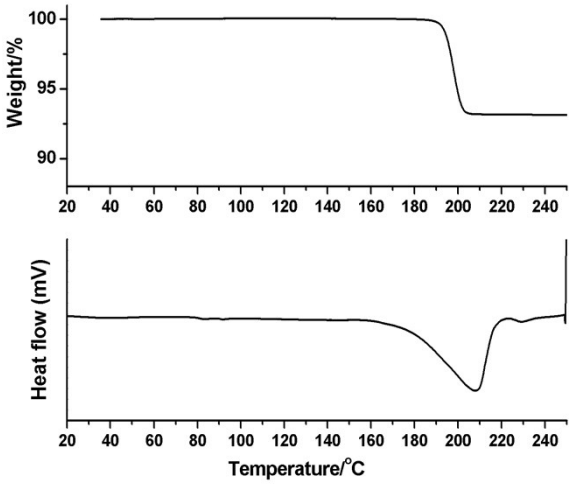

(a) Complex **3**

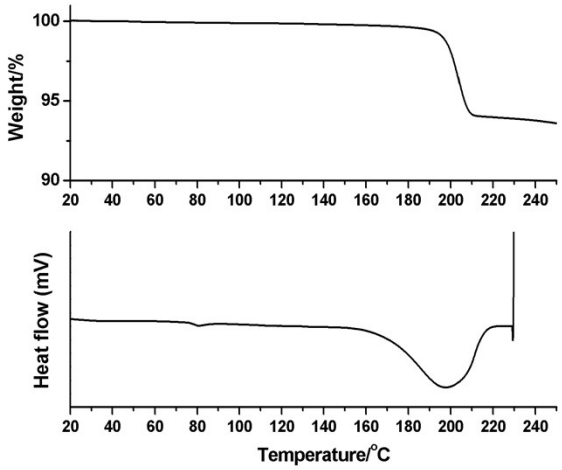

(b) Complex **4**

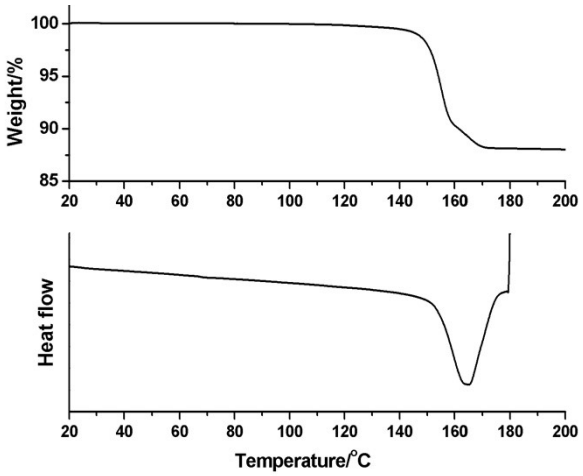

(c) Complex **5**

Fig. S8 Comparison of TGA (top) and DSC curves for the complexes **3–5**.

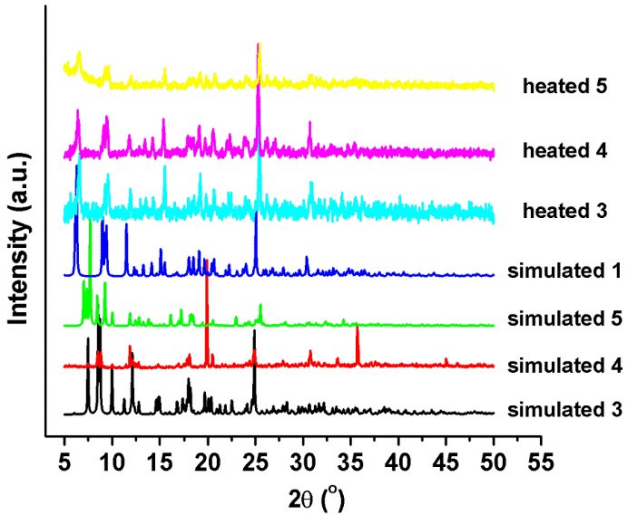

Fig. S9 Comparison of the simulated (complex **1** and **3–5**) and measured (the heated samples of **3-5**) PXRD patterns.

Section 4: Diffuse Reflectance and Photoluminescence Properties

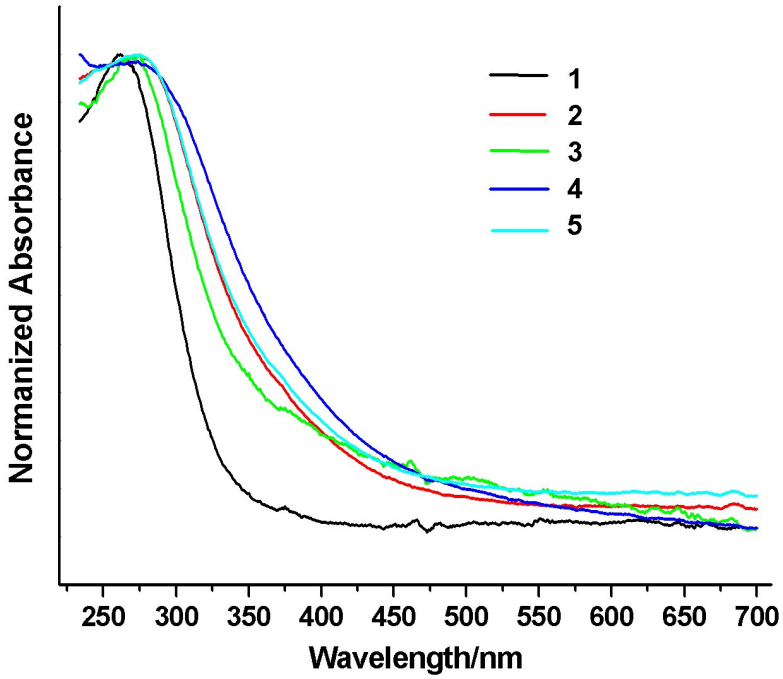

Fig. S10 Solid-state UV-Vis diffuse reflectance spectra at room temperature for the complexes **1–5**.

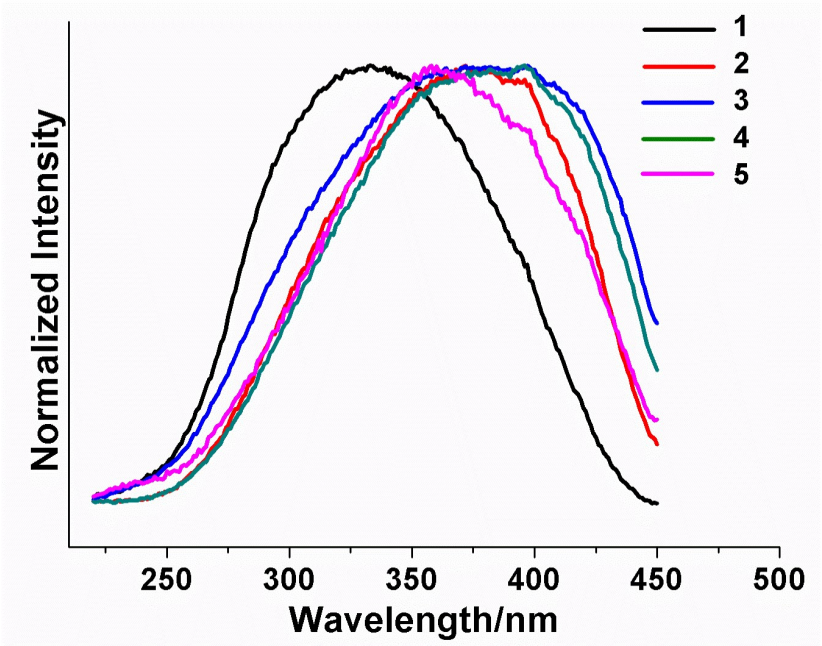

Fig. S11 Solid-state excitation spectra monitored at the corresponding emission maxima at room temperature for the complexes **1–5**.

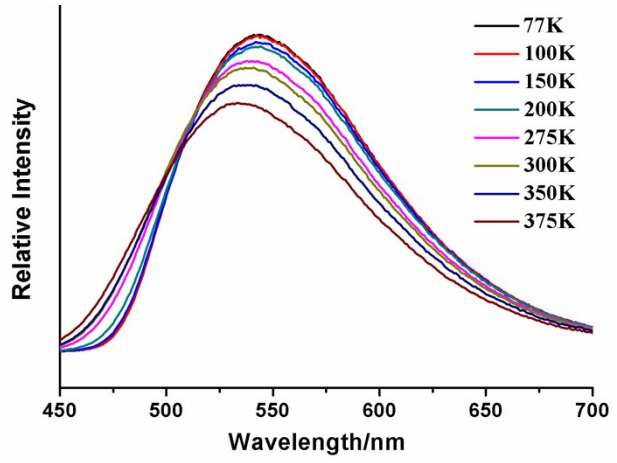

(a) Complex **1**

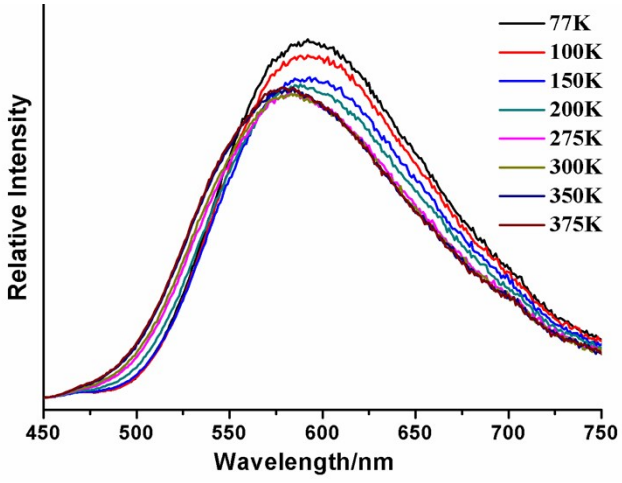

(b) Complex **2**

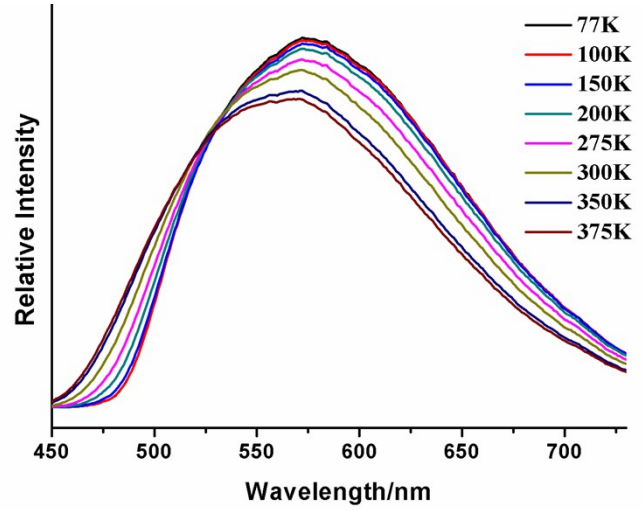

(c) Complex **3**

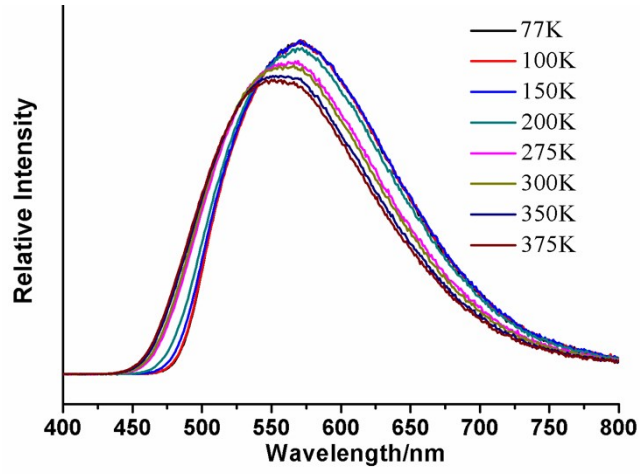

(d) Complex **4**

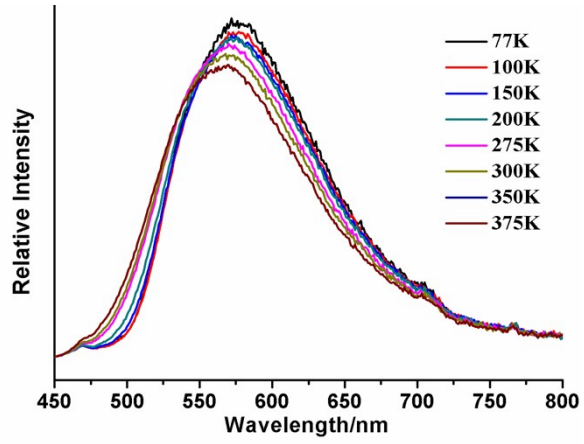

(e) Complex **5**

Fig. S12 Solid-state luminescence spectra upon various temperatures from 77 to 375 K for the complexes **1–5**.

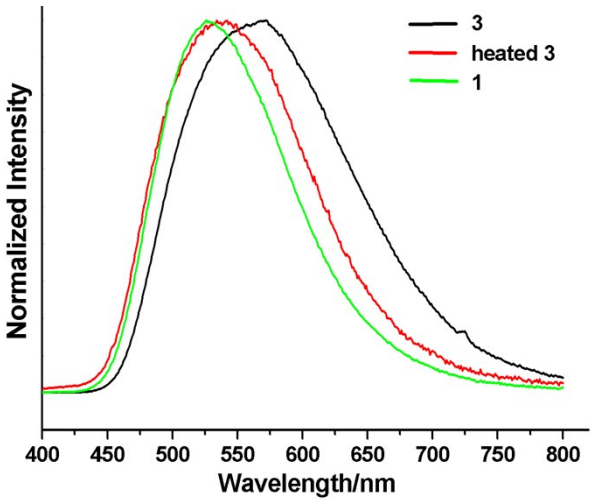

(a) Complex **3**

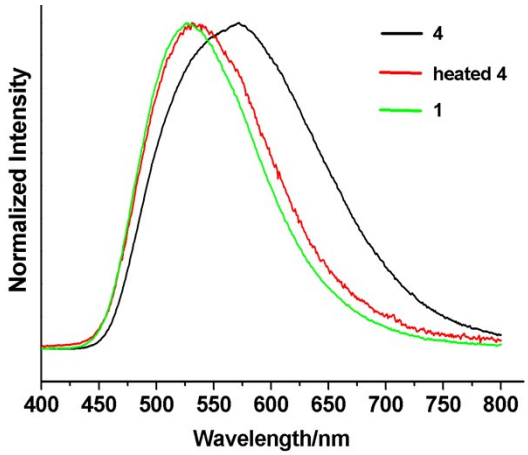

(a) Complex **4**

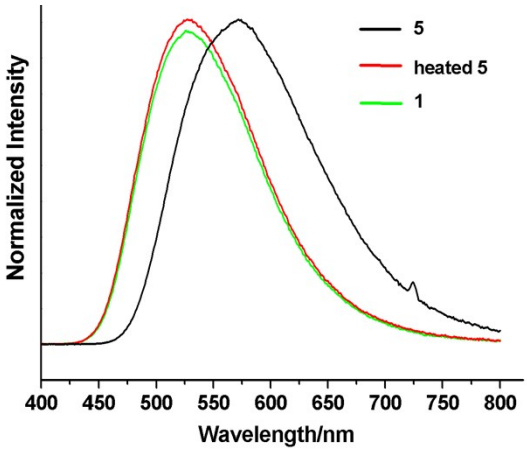

(a) Complex **5**

Fig. S13 Comparison of photoluminescence spectra of complex **1** with complex **3–5** and their heated samples

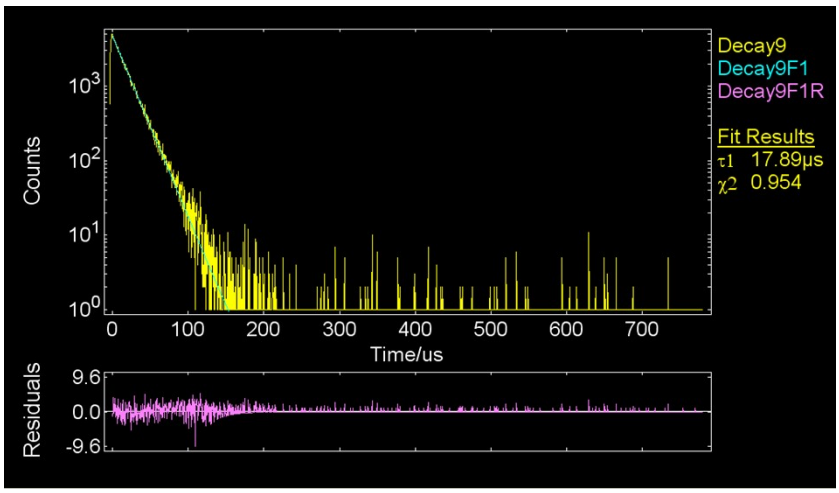

(a) Complex **1**

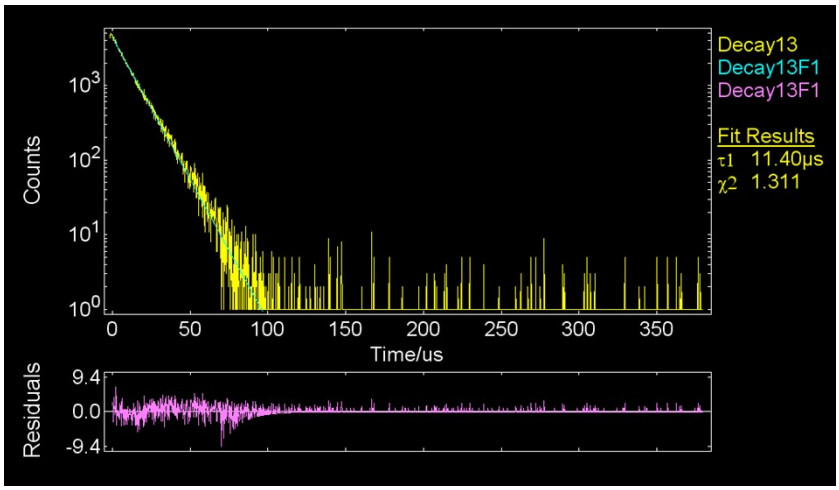

(b) Complex **2**

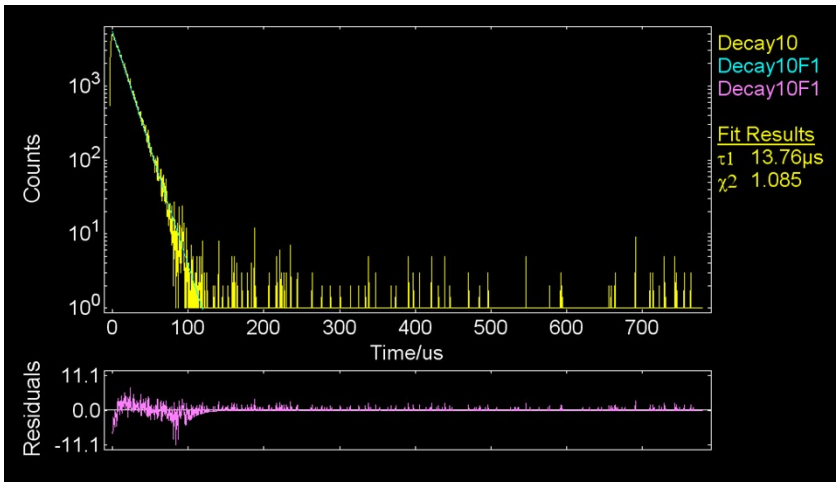

(c) Complex **3**

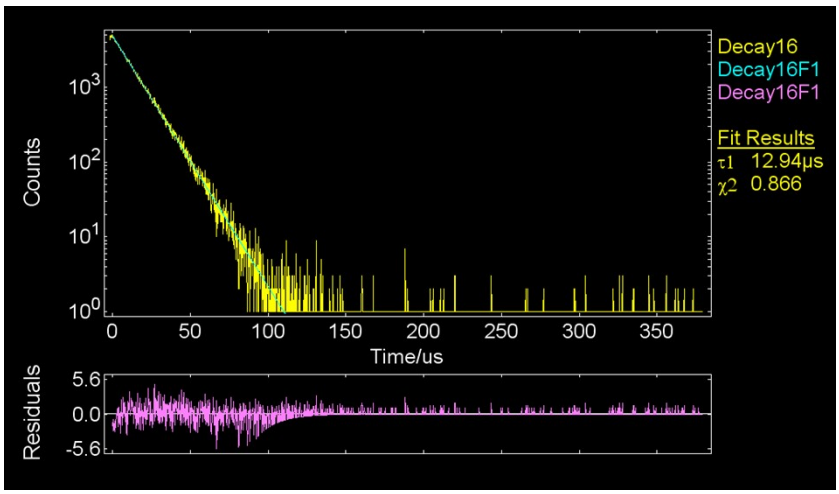

(d) Complex **4**

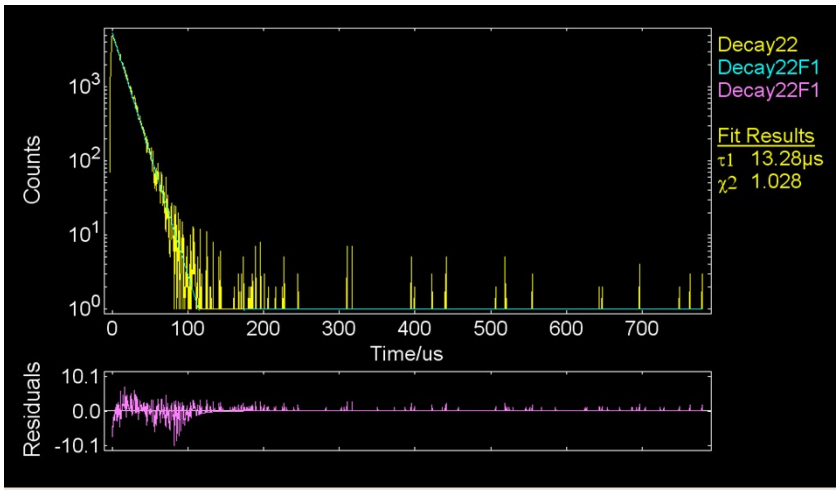

(e) Complex **5**

Fig. S14 Luminescence decay curves of the complexes **1–5** monitored at corresponding excitation/emission maxima.

Section 5: Density Functional Theory (DFT) Calculations

Unoptimized structure of a dimeric unit associated by N_{Py}···Cu weak coordination bonds in the complex **1** was used as a calculated model. All the calculations were carried out with Gaussian 09 software package,[S2] and some of the output files were used as input files of Multiwfn software packages[S3] to perform wave function analysis. PBE0 functional[S4-S6] was used throughout, LANL2DZ basis set[S7] was used for Cu atoms while the 6-31G** basis set[S8] was employed for other atoms (C, N, S and H). Hirshfeld composition was analyzed by Multiwfn software packages.[S9]

Electron density difference (EDD) maps could be obtained to provide accurate assignments of excited states by calculating singlet-singlet spin-allowed and singlet-triplet spin-forbidden transitions and then further treating the results by Multiwfn software packages.[S9]

Table S3 The calculated absorption spectra, the electron density difference (EDD) maps and the orbital transitions of the selected vertical singlet excited states for the calculation model (isovalue = 0.0004 a.u.).

Excited states	λ(nm)	*f*	Major transitions H = HOMO L = LUMO	Contribution(%) (>4.0)	EDD
S1	294	0	H→L H-1→L+1	65.53 27.70	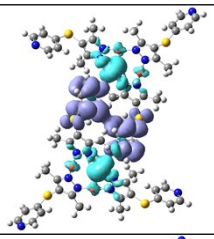
S2	293	0.0197	H-1→ L+1 H→ L+1	60.56 31.93	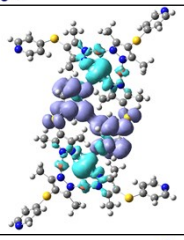
S3	277	0.0739	H→ L+2 H-1→ L+3 H → L+8 H-1→ L+9	39.92 24.50 15.44 8.69	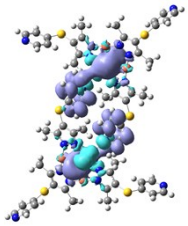
S4	277	0	H-1→ L+2 H-1→ L+8 H → L+3 H → L+9	34.23 15.99 27.41 10.09	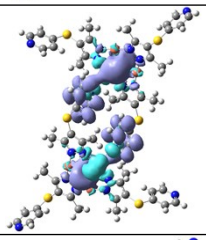
S5	269	0.0510	H-2→ L H → L+1 H-1→ L H-1→ L+2	31.17 12.91 7.66 7.49	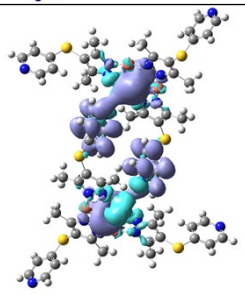
S6	268	0	H-3 → L H-1→ L+1 H-7→ L H-2→ L+1 H → L	35.30 8.63 7.77 7.61 5.36	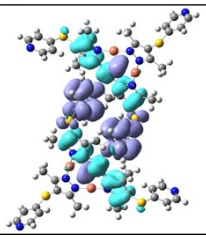

S7	268	0.0541	H → L+8 H → L+2 H-1→ L+9 H-2→ L	19.81 19.29 18.98 16.78	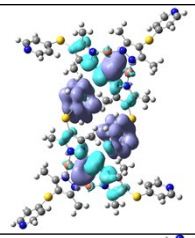
S8	267	0	H → L+9 H-1→ L+2 H-1→ L+8 H-3 → L	26.81 26.36 21.49 5.13	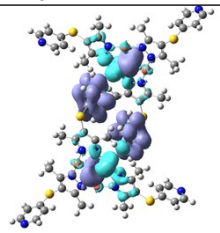
S9	267	0	H-1→ L+1 H → L	50.53 22.31	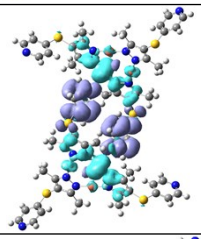
S10	267	0.0166	H → L+1 H-1→ L	44.59 23.02	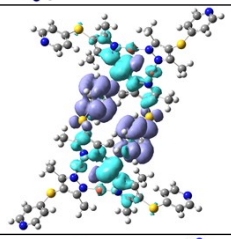
S20	252	0.02	H-6→ L H-5→ L H-7→ L+1 H-2→ L H-1→ L+3	19.78 10.21 7.78 7.09 5.84	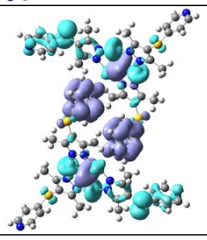

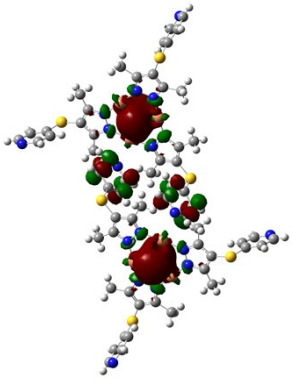

LUMO+9

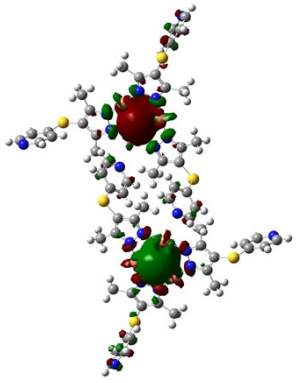

LUMO +8

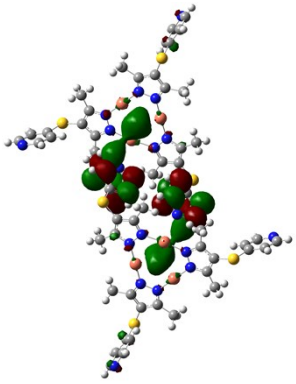

LUMO +3

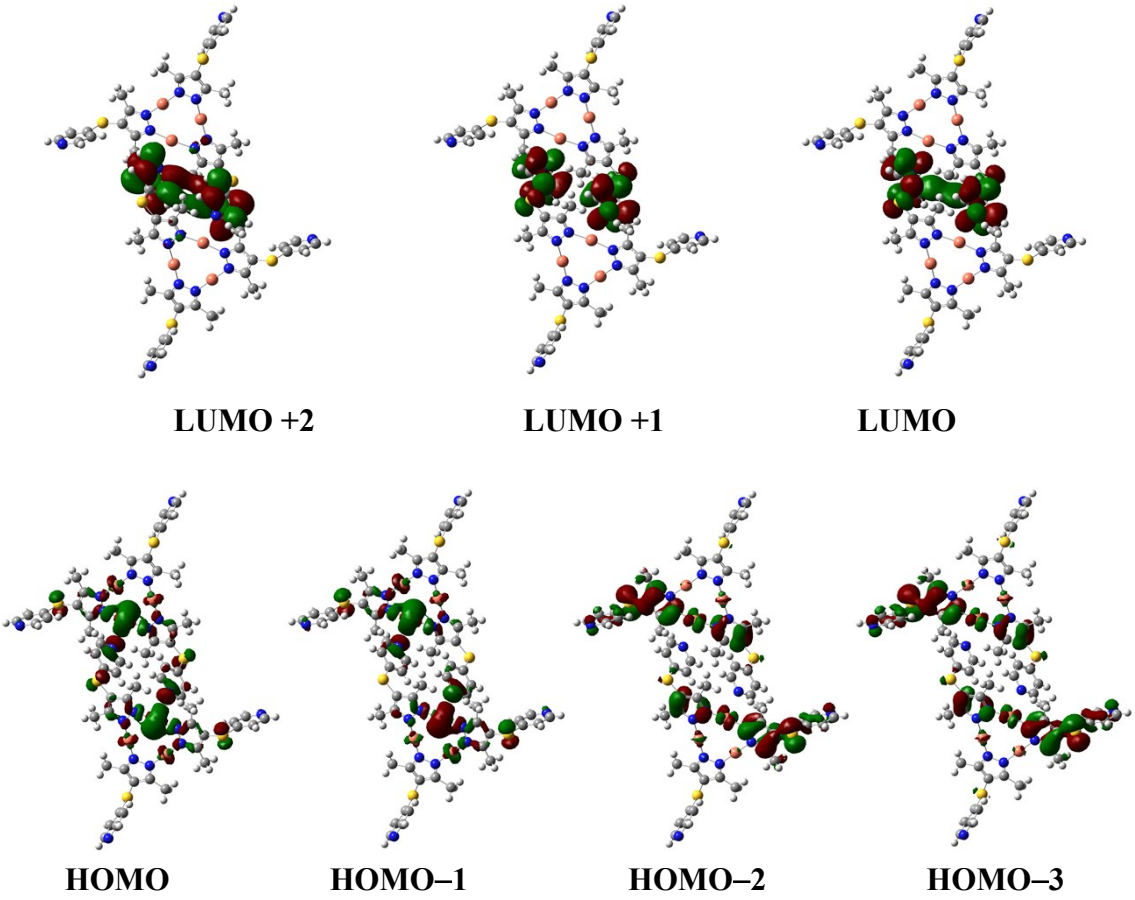

Fig. S15 Selected molecular orbitals (MOs) at the PBE0 level of theory for the calculated model (isovalue = 0.0004 a.u.).

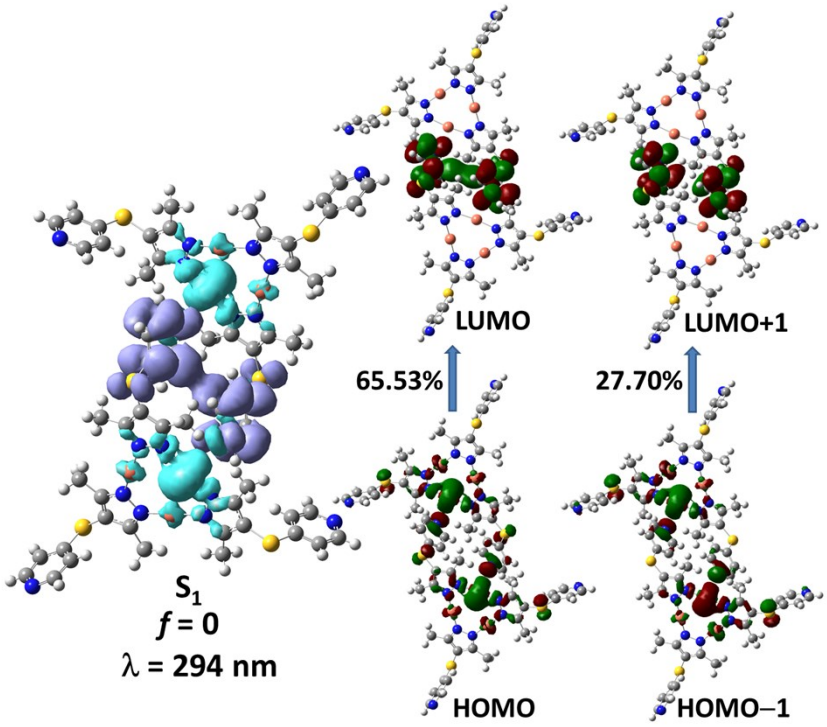
LUMO
LUMO+1
65.53%
27.70%
S1
f = 0
λ = 294 nm
HOMO
HOMO−1

(a)

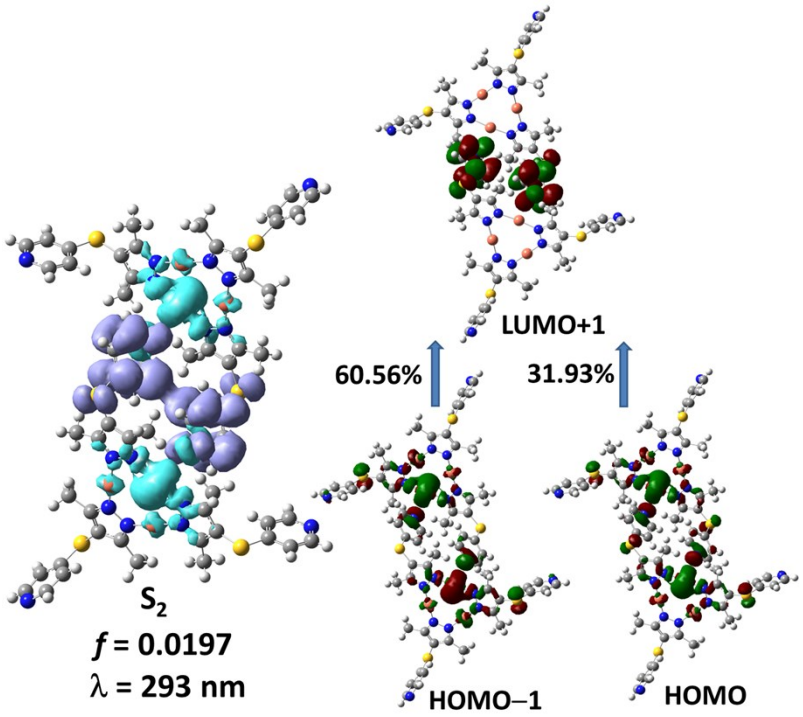
LUMO+1
60.56%
31.93%
S2
f = 0.0197
λ = 293 nm
HOMO−1
HOMO

(b)

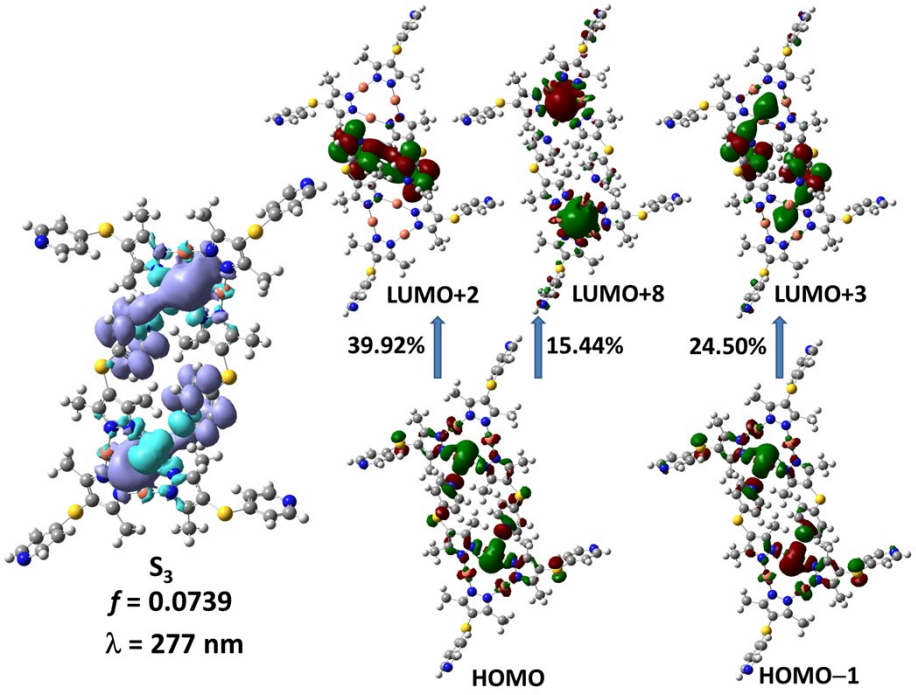
LUMO+2
LUMO+8
LUMO+3
39.92%
15.44%
24.50%
S3
f = 0.0739
λ = 277 nm
HOMO
HOMO−1

(c)

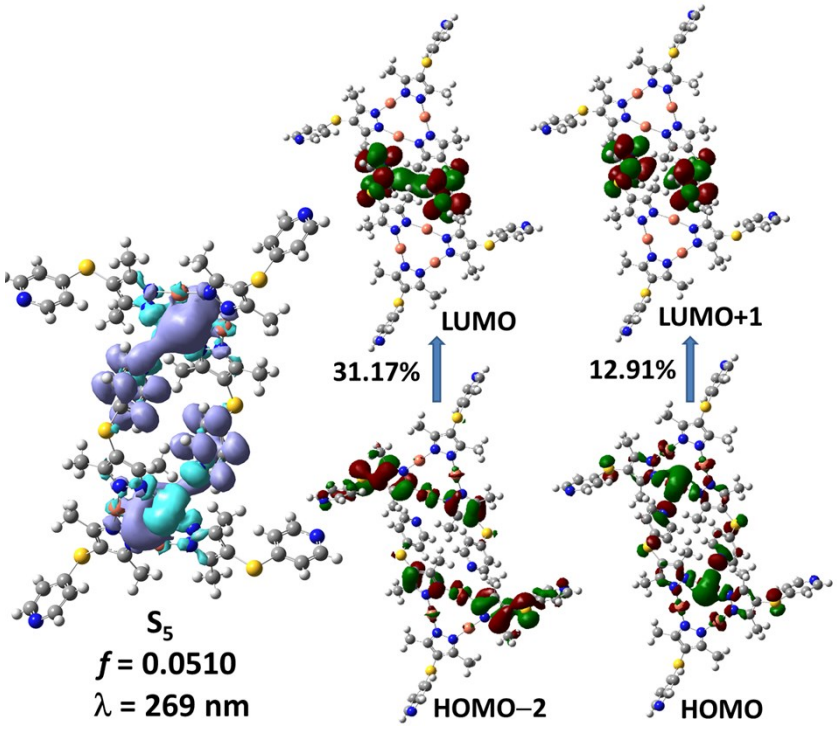
LUMO
LUMO+1
31.17%
12.91%
S5
f = 0.0510
λ = 269 nm
HOMO−2
HOMO

(d)

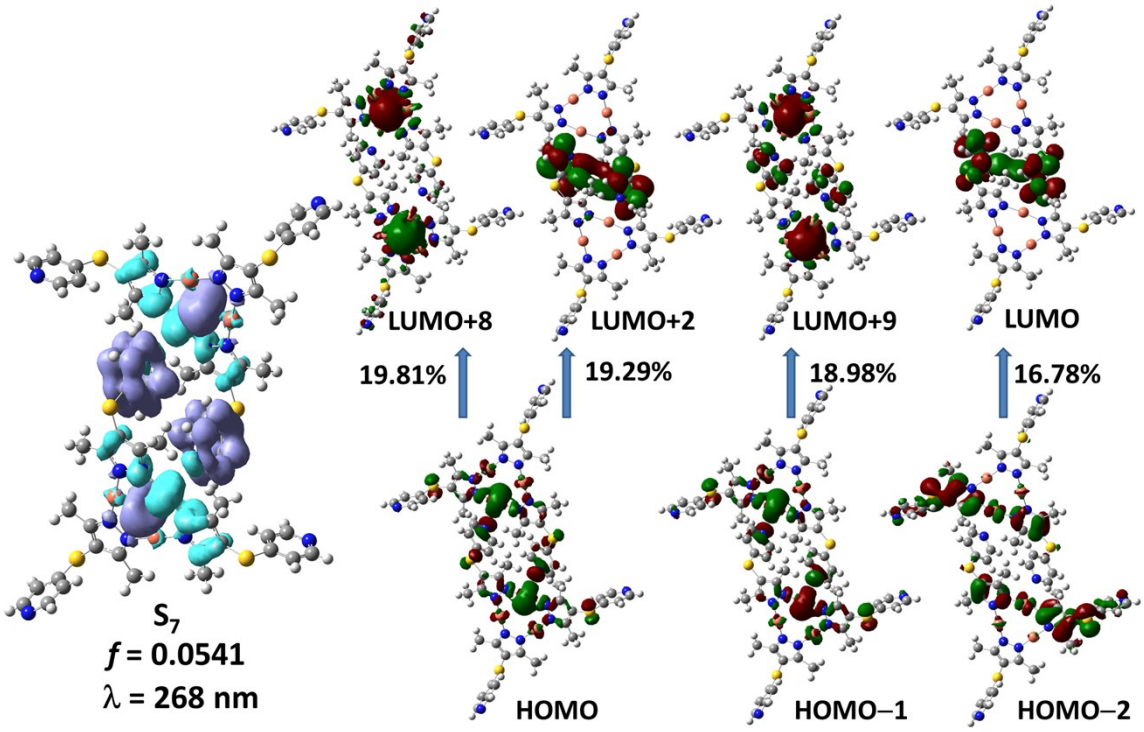

(e)

Fig. S16 Electron density difference maps (left, density transferring from the part in cyan to purple) of the selected singlet excited states of S_1 (a), S_2 (b), S_3 (c), S_5 (d), S_7 (e) marked with oscillator strengths *f* and energy levels for the dimeric unit associated by N_{Py}···Cu weak coordination bonds, and spatial plots of the selected molecular orbitals (right) involved in these singlet state transitions (isovalue = 0.0004 a.u.).

References

S1 G. M. Sheldrick, *Acta Crystallogr., Sect. A: Found. Crystallogr.* **2008**, *64*, 112.

S2 M. J. Frisch, G. W. Trucks, H. B. Schlegel, G. E. Scuseria, M. A. Robb, J. R. Cheeseman, G. Scalmani, V. Barone, B. Mennucci, G. A. Petersson, H. Nakatsuji, M. Caricato, X. Li, H. P. Hratchian, A. F. Izmaylov, J. Bloino, G. Zheng, J. L. Sonnenberg, M. Hada, M. Ehara, K. Toyota, R. Fukuda, J. Hasegawa, M. Ishida, T. Nakajima, Y. Honda, O. Kitao, H. Nakai, T. Vreven, Jr. J. A. Montgomery, J. E. Peralta, F. Ogliaro, M. Bearpark, J. J. Heyd, E. Brothers, K. N. Kudin, V. N. Staroverov, R. Kobayashi, J. Normand, K. Raghavachari, A. Rendell, J. C. Burant, S. S. Iyengar, J. Tomasi, M. Cossi, N. Rega, J. M. Millam, M. Klene, J. E. Knox, J.B. Cross, V. Bakken, C. Adamo, J. Jaramillo, R. Gomperts, R. E. Stratmann, O. Yazyev, A. J. Austin, R. Cammi, C. Pomelli, J. Ochterski, R. L. Martin, K. Morokuma, V. G. Zakrzewski, G. A. Voth, P. Salvador, J. J. Dannenberg, S. Dapprich, A. D. Daniels, O. Farkas, J. B. Foresman, J. V. Ortiz, J. Cioslowski, D. J. Fox, GAUSSIAN 09 (Revision A.02), Gaussian, Inc., Wallingford, CT, 2009.

S3 T. Lu, F. W. J. Chen, *Comp. Chem.* 2012, **33**, 580.

S4 J. P. Perdew, K. Burke, M. Ernzerhof, *Phys. Rev. Lett.* 1996, **77**, 3865.

S5 J. P. Perdew, K. Burke, M. Ernzerhof, *Phys. Rev. Lett.* 1997, **78**, 1396.

S6 C. Adamo, V. Barone, *Theor. Chem. Acc.* 2000, **105**(**2**), 169.

S7 P. J. Hay, W. R. Wadt, *J. Chem. Phys.* 1985, **82**, 270.

S8 J. E. Del Bene, *Chem. Phys. Lett.* 1983, **94**(**2**), 213.

S9 Multiwfn manual, version 3.3.8, http://multiwfn.codeplex.com/.